



RAPID COMMUNICATION

Interconnected carbon nanotube/graphene nanosphere scaffolds as free-standing paper electrode for high-rate and ultra-stable lithium-sulfur batteries



Lin Zhu^{a,b,1}, Hong-Jie Peng^{b,1}, Jiyuan Liang^c, Jia-Qi Huang^{b,n},
Cheng-Meng Chen^d, Xuefeng Guo^c, Wancheng Zhu^{a,n}, Peng Li^e,
Qiang Zhang^{b,n}

^aDepartment of Chemical Engineering, Qufu Normal University, Shandong 273165, China

^bBeijing Key Laboratory of Green Chemical Reaction Engineering and Technology, Department of Chemical Engineering, Tsinghua University, Beijing 100084, China

^cKey Laboratory of Mesoscopic Chemistry, School of Chemistry and Chemical Engineering, Nanjing University, Nanjing 210093, China

^dKey Laboratory of Carbon Materials, Institute of Coal Chemistry, Chinese Academy of Sciences, 27 Taoyuan South Road, Taiyuan 030001, China

^eBeijing Tsingna Technology Co., Ltd, Beijing 100084, China

Received 12 October 2014; received in revised form 26 November 2014; accepted 27 November 2014

Available online 9 December 2014

KEYWORDS

Flexible electrodes;
Lithium-sulfur batteries;
Carbon nanotubes;
Graphene

Abstract

The rational design and fabrication of flexible electrodes with high capacity, high rate capability, and high cycling stability is of urgent need for bendable, wearable, and implantable electronic devices. The integration of conductive nanocarbon as flexible scaffolds is an efficient and effective route toward flexible high-energy-density lithium-sulfur batteries. Herein, a free-standing paper electrode was constructed by rational integration of high conductive super-long carbon nanotubes (CNTs) and nano-sized hollow graphene spheres (GSs) through a room-temperature solution-processable method for lithium-sulfur batteries. The hollow GSs afforded close space to accommodate sulfur species, sustain the volume fluctuation during cycling, and retard the dissolution of polysulfides and parasitic shuttle. The graphene walls of GSs and super-long CNTs synergistically constructed hierarchical short-/long-range electron/ion pathways.

ⁿCorresponding authors.

E-mail addresses: jqhuang@tsinghua.edu.cn (J.-Q. Huang), zhuwancheng@tsinghua.org.cn (W. Zhu), zhang-qiang@mails.tsinghua.edu.cn (Q. Zhang).

¹Both authors contributed equally to this work.

Consequently, the as-obtained flexible paper electrode was with a high sulfur utilization of 81% (corresponding to 1346 mA h g^{-1}) at a current density of 0.17 A g^{-1} (0.19 mA cm^{-2}), a high-rate capacity retention of 40% when the current density increased to supreme 16.7 A g^{-1} (18.4 mA cm^{-2}), and a superior capacity retention of 89.0% over 500 cycles. This proof-of-concept research indicated the well hybridization of graphene and CNTs holds promise in the efficient use as flexible electrodes for future flexible electronics.

& 2014 Elsevier Ltd. All rights reserved.

Introduction

The commercial success of flat-panel displays starts an era of flexible electronics, leading to their new applications in rollable displays [1]. Other promising applications, including thin film solar cells, touch screens, wearable sensors, implantable medical devices, artificial skins, conformable active radio-frequency identification tags, and sensors, have attracted intensive interest in building electronic devices directly on flexible substrates. Driven by the growing demand for electronics permitting lightweight design, portability, and low manufacturing cost, the flexible electronics have been highly concerned by scientific communities as well as material and electronic industries [1-4]. However, these flexible electronics cannot be realized unless corresponding power sources are developed.

Lithium-ion batteries dominate the current portable device market due to their high energy density, high output voltage, long life, and environmentally friendly operation. However, currently the most commonly used rechargeable batteries are still too heavy, thick, rigid, and bulky to match practical requirements of flexible devices [3]. Advanced flexible electrochemical energy storage systems with various sizes, shapes, and mechanical properties are urgently required for the development of bendable, wearable, and implantable electronic devices. The key challenge to realize flexible batteries is to design and fabricate energy materials with high capacity, high rate capability, cycling stability, good conductivity, and robust flexibility, coupled with high performance electrolytes and separators in a rational assembly [3,5].

Lithium-sulfur batteries with a theoretical energy density of 2600 W h kg^{-1} have attracted great attentions as a promising candidate for flexible power sources [6,7]. The sulfur electrode possesses valuable characteristics of low equivalent weight, high capacity, low cost (around $150 \text{ \$ t}^{-1}$), and nontoxicity. However, the insulating nature of sulfur and lithium sulfide, the volume fluctuation during cycling, and the shuttle mechanism induced by the dissolution and diffusion of polysulfide intermediates hinder the full utilization of sulfur in a cell. The introduction of nanocarbon and/or conductive polymer scaffolds into sulfur cathodes exhibited a remarkable improvement in the electrochemical performance [8-10]. For instance, carbon nanotubes (CNTs) with extraordinary electrical conductivity and robust mechanical properties rendered outstanding performance when serving as conducting agents [11-16]. Wrinkled graphene materials were effective scaffolds for lithium-sulfur batteries because of their high accommodation capability of sulfur and tunable surface properties [17-21]. According to the demand for a

high-performance flexible sulfur cathode towards ultimate flexible devices, a desirable scaffolds should be rationally designed with following "3H" characteristics: (1) high three-dimensional (3D) electrical conductivity of the whole cathode scaffolds; (2) high accommodation capability for the sulfur-containing compounds; and (3) high mechanical strength to withstand the volume fluctuation during repeated cycling. As a successful paradigm for "3H" feature, super-long CNTs were served as both adhesive binders and conductive agents for flexible paper cathode in a lithium-sulfur batteries with high areal capacity for their advances in long-range electron transport, electrolyte accommodation, and mechanical robustness [12-14]. However, the entrapment of the polysulfides in the flexible CNT paper, which is the key for high cycling stability, should be further improved. The incorporation of porous carbon into CNT framework is consequently considered to confine polysulfides and retard the shuttle effect. For instance, free-standing carbide-derived carbon/CNT/sulfur cathode with high in-plane conductivity and enhanced cycling stability have been firstly proposed and realized by Kaskel's group [22]. The microporous carbon nanofiber/CNT/sulfur paper reported by Yu and co-workers exhibited much better cycle performance and rate performance compared to CNT-free cathode [23]. The micro-sized spherical porous carbon/CNT/sulfur composites with a high tap density and high sulfur content were successfully fabricated by Wang and co-workers to reduce the resistance of the composite and to improve the performance of lithium-sulfur batteries at high areal current densities [24]. Free-standing electrodes with rational pore structures and conducting networks by the in-situ assembly of CNTs and mesoporous carbon nanocages have been explored by our group [25]. Except for super-long CNTs, carbon fibers [26] and 3D graphene foam [27] also successfully served as current collectors with both 3D macropores to support huge amounts of sulfur and long-range electron paths. The rational design of the flexible cathode materials for "3H" high-capacity, high-rate, and high-stability lithium-sulfur batteries is still in extensive demand. Briefly, "3H" electrode and material design leads to "3H" energy-storage devices. The wise choice of sp^2 carbon building blocks and rational design of flexible electrodes based on CNT and graphene is the first step to fully demonstrate the "3H to 3H" idea and allow mechanistic insight on the energy chemistry based on nanomaterials.

To prove the "3H to 3H" concept, we employed super-long CNTs as the highly conductive network for long-range electron transfer and hollow graphene nanospheres (GS) as bifunctional building blocks to accommodate active sulfur and conduct the electron locally. The reason we selected hollow GS was aroused from its strong confinement of sulfur-containing compounds by the well-defined cavities

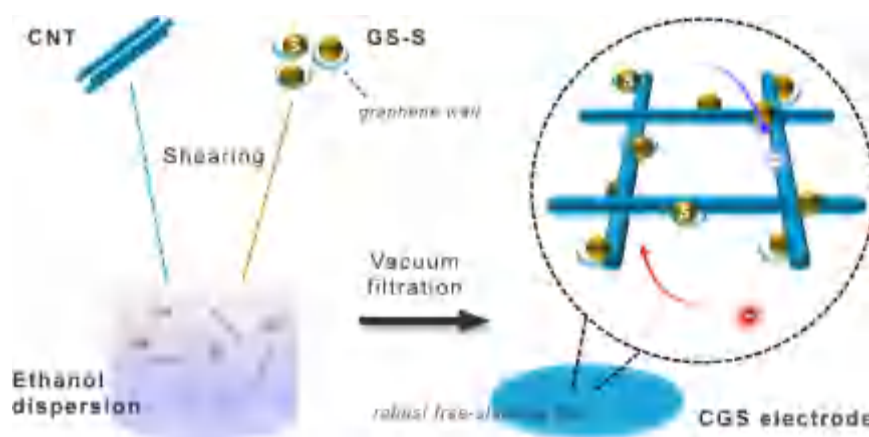


Fig. 1 Schematic of fabrication route for CGS electrode, including the ethanol co-dispersion of super-long CNTs and the GS-S, and the assembly into robust free-standing films through vacuum filtration.

and high electrical conductivity contributed by the sp^2 carbon shells. In addition, the super-long CNTs with superior flexibility and conductivity in composite electrodes also hold great potential in flexible electrode materials for lithium-ion batteries, such as CNTs interweaved Fe_3O_4 nanocrystals [28] and $Li_4Ti_5O_{12}/CNT$ nanostructure [29]. Based on these considerations, a shearing dispersion-filtration approach was employed to fabricate the flexible paper electrode (Fig. 1). The CNTs were dispersed in the sulfur saturated ethanol solution by vigorous shearing to de-bundle and then GS-S composite materials were added under shearing to obtain a uniformly mixture. Flexible CNT/GS-S (CGS) paper electrode was fabricated through the facile vacuum filtration method. The routine graphene flakes (GFs) were employed as the control sample to indicate the role of close space of GSs for the lithium ion storage performance in the flexible composite electrode. The as-obtained free-standing CGS electrode was expected with high discharge capacity and high rate performance in a lithium-sulfur cell.

Results and discussion

The 3D flower-like mesostructure of the GS building blocks was shown in Fig. 2a. The flower-like nanoarchitectures were assembled by highly curved thin flakes with a thickness of ca. 20–30 nm. Such two-dimensional (2D) nanosheets were composed of single-layer of hollow GSs with a diameter of 20–30 nm (see inset of Fig. 2a). The detailed nanostructures of the GSs were determined by the high resolution TEM (Fig. 2b). The size of hollow interior was around 15–30 nm, and the outer shell was of single-/few-layer nano graphene. The GS was with an I_D/I_G ratio of 1.40 according to Raman spectra, an oxygen content of 1.0 at% determined by X-ray photoelectron spectroscopy, and an electrical conductivity of 695 S m^{-1} obtained by four-probe analysis. In contrast, large-sized 2D GFs with open pore structure were selected as control sample. As shown in Fig. 2c and d, GFs were thermally exfoliated from graphene oxide with a lateral size of several to several tens micrometer. The GFs were with an I_D/I_G ratio of 1.44, an oxygen content of 2.9 at%, and an electrical conductivity of 276 S m^{-1} . The pore structures of GS and GF

were elucidated by the N_2 sorption isotherms and corresponding pore size distributions (Fig. 3a). The GS and GF possess specific surface area of 979 and $685\text{ m}^2\text{ g}^{-1}$, a pore volume of 1.98 and 2.14 mL g^{-1} , respectively. Benefiting from the nanosized hollow cavity and the single-/few layer nature of graphene walls, the GSs presented much higher specific surface area and abundant 5–20 nm mesopores than these of GFs. Therefore, the GS building blocks can (1) accommodate higher sulfur loading amount and sustain the volume fluctuation, (2) afford interlinked electron transportation network from CNTs to active sulfur, and (3) provide interconnected 3D nanopores as lithium ion pathways for high-rate electrochemistry.

After the routine but facile co-heating procedure for carbon/sulfur composite fabrication, the sulfur was successfully immersed into the pores of GSs and GFs to form GS-S and GF-S composites under vacuum without obvious morphological change and formation of large sulfur particles (Fig. S1). The amount of sulfur in GS-S was determined to be 64 wt% by thermogravimetric analysis (TGA) in N_2 atmosphere (Fig. S2). The weight loss peak of sulfur in GS-S shifted to a temperature range of 200–350 °C, which was higher than that of element sulfur. In the ultimate solution-processed CGS and CNT/GF-S (CGF) film electrode, the apparent decrease of pore volume as well as the specific surface area reconfirmed that the electrochemically active sulfur was accommodated into the pores of graphene (Fig. S3). Furthermore, a certain amount of pores structure was remained after a 64% sulfur loading to GS. However, in terms of GF, the representative hysteresis loop of mesopore structure almost disappeared after the sulfur incorporation with the same ratio. The detailed structures were also checked by the X-ray diffraction (XRD) (Fig. 3b). The sulfur phase in the GS-S and GF-S composite were of poor crystallization, indicating the uniform distribution of ultrafine sulfur in the graphene/sulfur composite. Even after vigorous shearing in saturated sulfur solution in ethanol with CNTs, sulfur particles retained its small size and no recrystallization of sulfur into large particles were observed. Actually, the sulfur content in the ultimate film electrode was in good accordance with the mass ratio of CNTs and graphene/sulfur composites. This can be attributed to the hydrophobic sp^2 carbon surface that poses a strong coupled interface

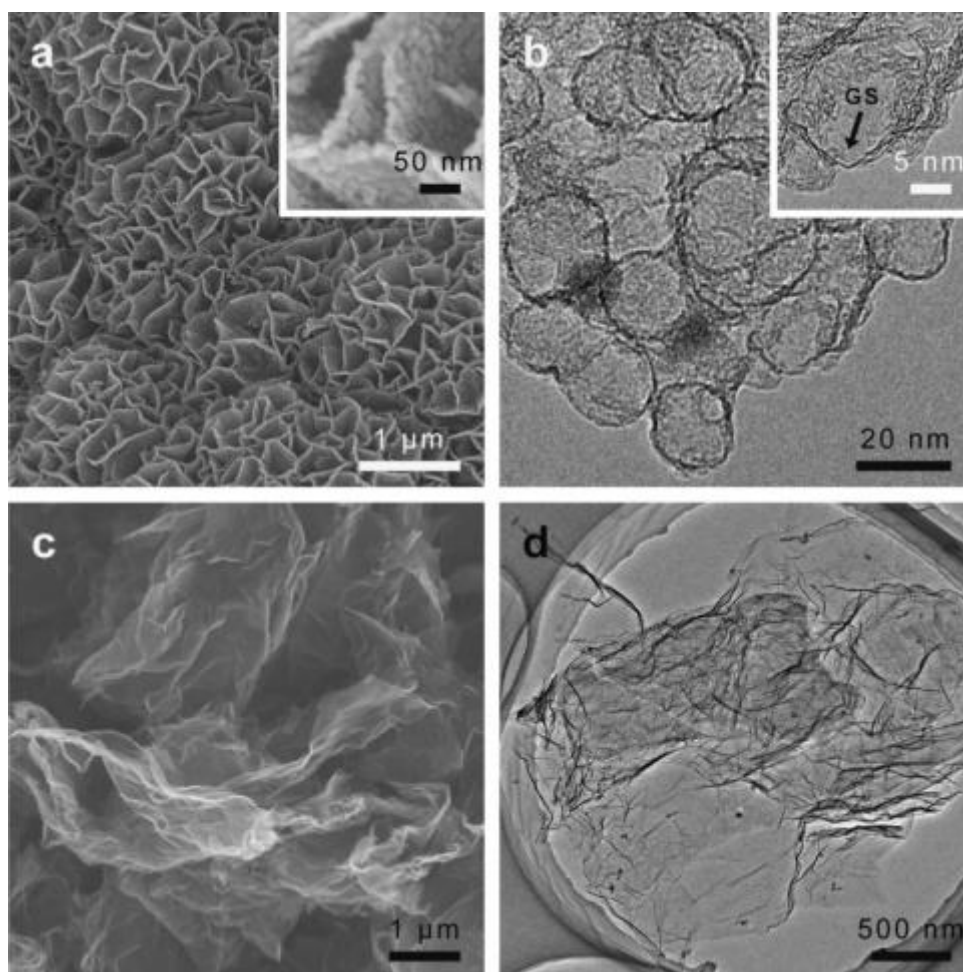


Fig. 2 Morphology of GS and GF units: (a) SEM image of GS (inset shows enlarged HR-SEM image), (b) TEM image of GS (inset is HRTEM showing GS walls), (c) SEM image of GF, (d) TEM image of GF.

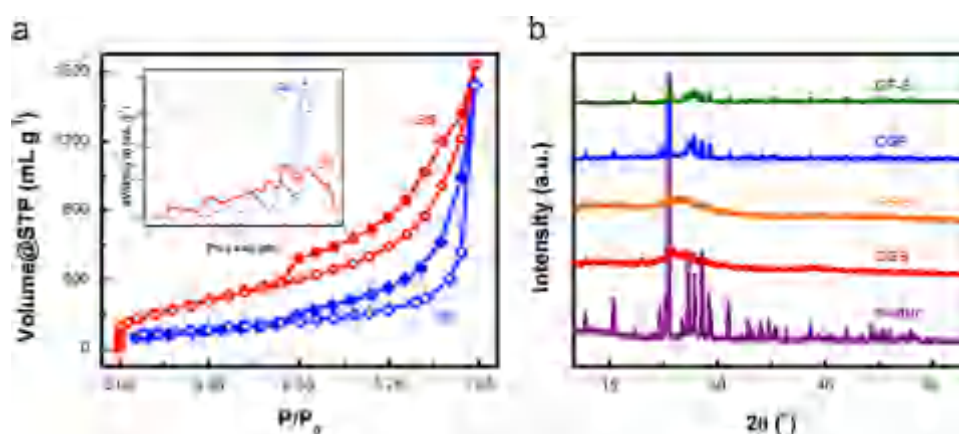


Fig. 3 (a) N_2 isothermal adsorption and corresponding pore size distribution results of GS and GF; (b) XRD patterns of GS-S, CGS paper, GF-S, CGF paper, and sulfur.

to attach the non-polar sulfur molecules [30]. Note that CGS exhibited much weaker diffraction of sulfur than CGF, indicating smaller sulfur phase domain in CGS. Thus, higher utilization of active materials for CGS was expected.

The GS-S and GF-S composites were uniformly distributed into super-long CNT scaffolds as paper electrodes fabricated by the facile vacuum filtration route. The digital image of CGS

flexible membrane was shown in Fig. 4a. The areal sulfur loading amount in the electrode reached 1.1 mg cm^{-2} , which was higher than the routine doctor blade method [11,21,31]. Despite the high loading, the CNT/graphene hybrid interlinked structure ensured the mechanical strength of the sulfur-containing flexible film due to the extraordinary inherent mechanical strength of CNTs [26] and robust hydrophobic

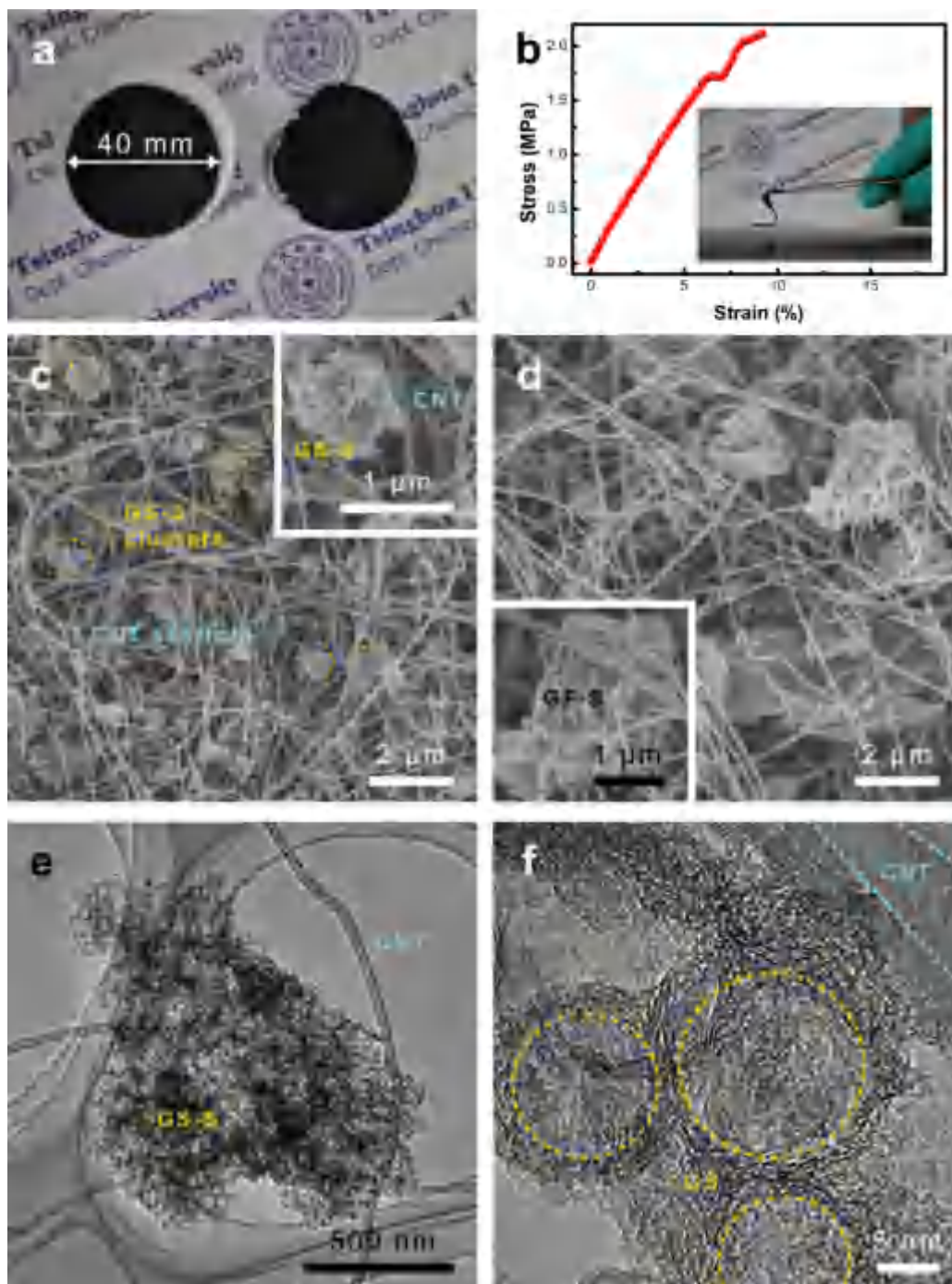


Fig. 4 (a) Digital photograph of CGS paper after peeling off; (b) strain-stress profile of CGS paper and its bending state (inset); (c) SEM images of CGS (inset is enlarged view), (d) SEM images of CGF paper (inset shows enlarged view), (e) TEM and (f) HR-TEM images of CGS structure.

assembly (Fig. 4b). An outstanding robustness was indicated by the high strength of 2.1 MPa at strain of 9.3%.

In order to reveal the detailed nanostructure, the morphologies of the flexible CGS cathode were elucidated by scanning electron microscopy (SEM) and transmission electron microscopy (TEM). The 2-mm-long CNTs fabricated by the floating catalyst method (Fig. S4) were applied the flexible scaffolds. During the vigorous shearing in polar solvent, the aligned CNTs de-bundled along its c-axis and formed intercrossed networks

for sulfur-storage units. As shown in Fig. 4c, the GS-S clusters were uniformly distributed and intimately decorated among the CNT networks. Even suffering from severe ultrasonication, a GS-S cluster was still linked with super-long CNTs (Fig. 4e). Close contacts between CNTs and GSs were further confirmed by the TEM image (Fig. 4f), which allowed rapid electron transference through the hierarchical conducting networks. In contrast, less contact sites or junctures were available between CNTs and graphene in CGF, which was mainly ascribed

to the large lateral size of GFs (Fig. 4d). Hence repeated dissolution and re-deposition of sulfur species onto the GF planes might hinder such fragile connection between GFs and CNTs and then induced performance degradation as well. While the design of CGS flexible electrode fully inherited the advantages of outstanding long-range electrical conductivity of CNTs and close confinement in hollow interior of GSs. On one hand, the super-long CNTs served as (1) 3D interlinked current collector for long range electron transfer, (2) adhesive binder to attach GS-Ss, and (3) macroporous robust network to allow deep penetration of electrolyte and to prevent segregation of sulfur particles. On the other hand, the GSs serve as (1) the short-range electron transfer pathway with intimate contact with CNT network, (2) reservoir for sulfur, polysulfides, and lithium sulfides, and (3) protecting shell to buffer volume change. The derived hybrid film possessed a high electrical conductivity of 17.9 S cm^{-1} . Therefore, a multifunctional, hierarchical, hybrid CNT/graphene-based carbon structure was achieved to meet both the demand for flexible devices and high-performance lithium-sulfur batteries.

Both the CGS and CGF were employed as flexible cathodes in lithium-sulfur cells. The cyclic voltammetry (CV) was conducted to investigate the electrochemical behavior of CGS flexible cathode at a scan rate of 0.1 mV s^{-1} in the voltage range from 1.6 to 3.0 V. As shown in Fig. S5, two main reduction peaks at around 2.03 and 2.31 V was clearly presented during the first cathodic scan, which corresponded to the reduction of element sulfur to lithium polysulfides ($n\text{S} + 2\text{Li}^+ + 2\text{e}^- \rightarrow \text{Li}_2\text{S}_n$, ($4r \text{ n r } 8$)) and the ultimate transformation of lithium polysulfides into lithium sulfides ($\text{Li}_2\text{S}_n + 2(n-1)\text{Li}^+ + 2(n-1)\text{e}^- \rightarrow n\text{Li}_2\text{S}$ ($n \geq 4$)), respectively [21]. Two oxidation peaks at 2.33 and 2.38 V in the subsequent anodic scan were also identified, which were correlated to the oxidation of lithium sulfide to lithium polysulfide and further conversion to element sulfur, respectively [21,25]. The reduction peaks were well maintained at the sequent cycles, and no obvious changes on the intensity and position of the peak in the process of cathodic scan were observed in the subsequent scanning cycles, indicating a good electrochemical reversibility of the CGS flexible electrode.

As illustrated in Fig. 5, the CGS electrodes possessed very high specific discharge capacities of 1346, 1155, 1024, 931, 827, and 606 mA h g^{-1} were achieved at current densities of 0.17, 0.34, 0.85, 1.67, 3.34, and 8.35 A g^{-1} , respectively. Even at a high current density of 16.7 A g^{-1} , a high reversible capacity of 535 mA h g^{-1} can still be preserved. Note that comparable high-rate performance was only available in the case of low sulfur loading amount ($\approx 50 \text{ wt\%}$ or $\approx 1.0 \text{ mg cm}^{-2}$) and low areal current density ($\approx 2.0 \text{ mA cm}^{-2}$) [27,28,32,33] while an unparalleled areal current density of 18.4 mA cm^{-2} was applied in our case. Moreover, a capacity of 1084 mA h g^{-1} was also obtained when the current density decreased from 16.7 to 0.17 A g^{-1} . As a comparison, the rate performance of CGF was evaluated with a similar sulfur loading amount. Although a high discharge capacity 1194 mA h g^{-1} was achieved at a low current densities of 0.17 A g^{-1} , it decayed sharply to 112 mA h g^{-1} when the current density increased to 3.34 A g^{-1} , which was only 9.4% of that at 0.17 A g^{-1} . Such comparison indicated the superiority of GS on high-power properties with much better connection and abundant transport sites.

The discharge capacity retention curves during 0.5 C ($1 \text{ C} = 1.67 \text{ A g}^{-1}$) cycling of CGS and CGF paper electrodes

were demonstrated as Fig. 5b. When the GS was used for the flexible CNT-based cathode, a supreme capacity retention of 95.9% and an ultralow decay rate of 0.02% per cycle for 200 cycles were achieved. In contrast, the capacity of CGF descended to 67.4% within only 50 cycles, which corresponded to a high decay rate of 0.54% per cycle. Fig. 5c described the long-term galvanostatic cycling performance CGS flexible cathode. An initial discharge capacity of 829 mA g^{-1} at 0.5 C was delivered with a voltage window of 1.8–2.8 V. Despite of a relatively high sulfur loading of 1.1 mg cm^{-2} , the capacity maintained well over 500 cycles, along with an extremely high retention of 97.8, 95.9, 92.8, 90.4, and 89.0% at 100, 200, 300, 400, and 500 cycles, and a high coulombic efficiency above 99%. The stable electrochemical characteristics of CGS cathode after 500 cycles were also validated by galvanostatic charge-discharge profiles (inset left of Fig. 5c). Such stability is much improved than other flexible electrodes based on CNT/S paper [12] and CNT/porous carbon paper [25]. Typical two-plateaus voltage profiles correspond to the two-step redox electrochemical process were observed with exhibited slight polarization and plateaus shrinkage over the long-term cycling, indicating a highly reversible and stable electrochemistry. Such a supreme cycling stability of CGS electrodes was attributed to (1) confining hollow interior of GSs to retard severe dissolution of polysulfides in the case of open-structured GFs, (2) compact nano graphene shells to sustain huge volume change and retain intimate electrical contact, and (3) both mechanically and chemically robust CNT scaffolds to form interconnected channels and allow full flux of electrolytes (inset right of Fig. 5c). Note that strategy of physical confinement cannot intrinsically prevent the dissolution of polysulfides. LiNO_3 was employed as electrolyte additive to protect lithium anode, prevent the side reaction between polysulfides and lithium anode, and therefore suppress the well-known shuttle effect.

The superior lithium ion storage performance of the free-standing CGS paper electrode was ascribed to (1) the nano-sized GSs with highly conductive nano graphene walls affording intimate contact to sulfur species, which guaranteed high utilization of 81% (corresponding to 1346 mA h g^{-1}) at a relatively high areal loading amount of 1.1 mg cm^{-2} and a current density of 0.17 A g^{-1} ; (2) the bifunctional hollow cavity of GSs retarding the dissolution of polysulfides and parasitic shuttle phenomenon [34–37] and offering enough space for volume expansion of active materials even with a high sulfur content of 64%; (3) hierarchical electron pathway of short-range graphene walls of the GS and long-range CNT backbones, as well as 3D interconnected pore structure as ion channels for rapid transportation, resulting in 40% retention when the current density increased from 0.17 to 16.7 A g^{-1} ; and (4) highly stable carbon materials in the CGS electrode with good mechanical properties and chemical inertness instead of polymeric binders and metal current collector, improving long-term durability. Meanwhile, the superiority of flexible binder-/current collector free electrodes also included attractive potential to improve the energy density of the whole device due to the employment of light-weight materials. The 3D architecture of flexible electrode can be further improved by rational design of the nanocarbon building blocks to create composite electrode with various sizes, shapes, and mechanical properties. Besides, conductive polymer such as

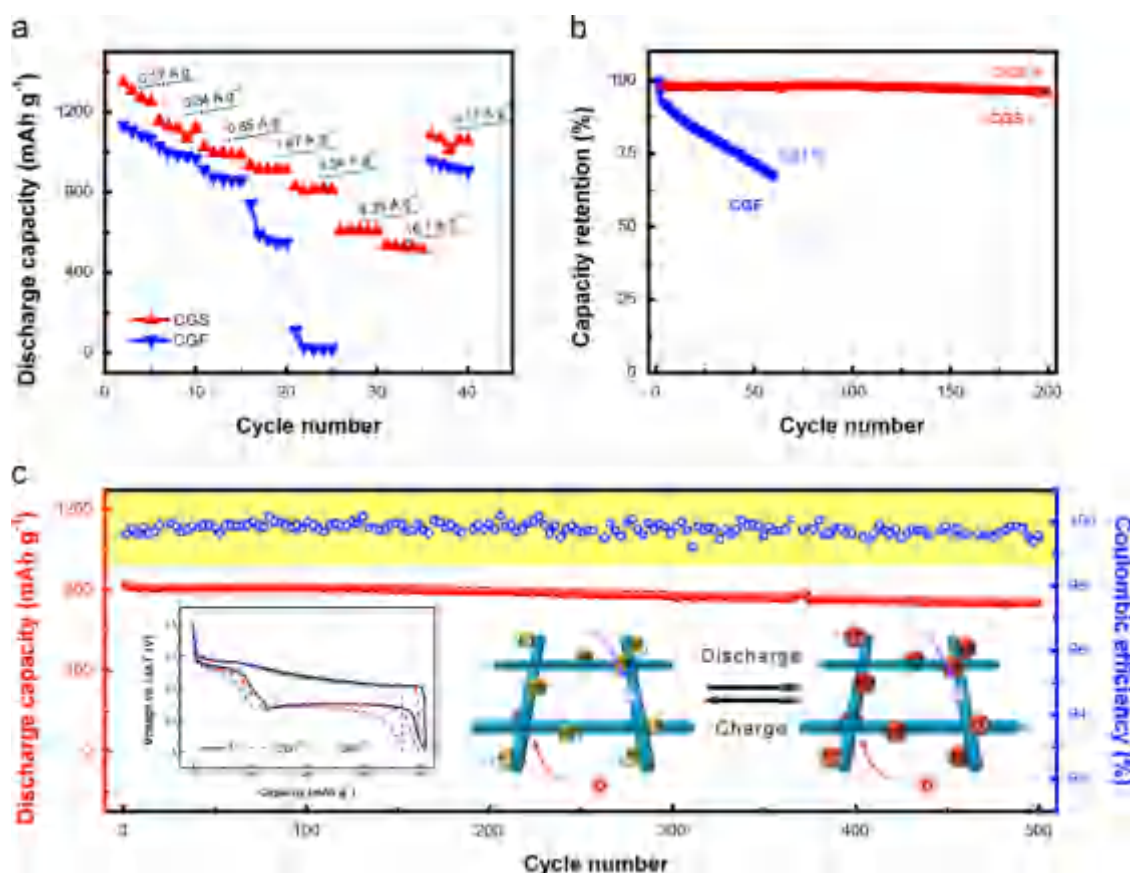


Fig. 5 Electrochemical performance: (a) rate performance and (b) capacity retention during 0.5 C cycling of CGS and CGF paper; (c) long-term cyclic test at 0.5 C (insets show galvanostatic discharge-charge curves of CGS paper).

polyacrylonitrile and polypyrrole are also a good platform for 3D sulfur cathode due to their feasible processibility and desirable chemical adsorption capability of sulfur species [26,38,39]. “3H” flexible lithium-sulfur batteries with high capacity, high rate capability, high cycling stability is highly expected with wise integration of CGS electrode with polysulfide reservoirs [38,40] and/or polysulfide diffusion inhibitor [29,41] in a cell.

Conclusions

A flexible CGS cathode was fabricated by hollow GSs and super-long CNTs through a room-temperature solution-processable method for lithium-sulfur battery. The super-long CNTs were employed to form highly efficient conductive networks and hollow GSs served as sulfur accommodation blocks. When CGS film was directly applied as electrodes, high specific discharge capacities of 1346, 1155, 1024, 931, 827, 606, and 535 mA h g^{-1} were achieved at different current densities of 0.17, 0.34, 0.85, 1.67, 3.34, 8.35, and 16.7 A g^{-1} , respectively. The CGS flexible cathode was with an ultra-low decay rate of 0.022% over 500 cycles and a high coulombic efficiency above 99% at a relatively high sulfur loading amount of 1.1 g cm^{-2} . Compared with the routine GFs, the well combination of hollow GSs with super-long CNTs afforded great advent to efficiently use the active materials. This proof-of-concept research indicated the importance of the rational design of the nanostructured

flexible electrode with “3H” feature of high capacity, high rate capability, and high cycling stability. Such procedure was also potentially applicable to integrate other building blocks as free-standing paper electrode for the ubiquitous applications of lithium-sulfur batteries, lithium ion batteries, supercapacitors, solar cells for future flexible electronic devices.

Experimental

Fabrication of GS-S & GF-S composite cathodes materials

The sulfur powder employed in this contribution with a purity of 499.9% was purchased from Alfa Aesar without further purification. The hollow graphene spheres was synthesized by a mesoscale approach reported in our previous publication [42]. A co-heating procedure was employed to accommodate the sulfur into the hollow space of the graphene spheres. Typically, sulfur powder was mixed with the GSs with a mass ratio of 7:3 in an agate mortar and strongly grinded for 10 min. The as-obtained GS-S mixtures were co-heated to 155 °C in a sealed quartz bottle. With a 4.0 h heating, the sulfur successfully immersed into the inner space of the spheres under vacuum and GS-S composite cathodes materials were available. The GF-S cathode was prepared in a similar procedure, except for that GF powder obtained by

the thermal reduction of graphene oxide [43] was employed as the carbon scaffolds.

Fabrication of CGS & CGF cathodes

The electrode of CGS was fabricated by a shearing dispersion-filtration method. In a typical reaction, 12.0 mg of super-long CNTs was dispersed in the sulfur saturated ethanol solution and kept shearing for 3.0 min in an ice bath. 28.0 mg of GS-S composite materials was added to above mentioned suspension and further sheared for another 1.0 min. The whole dispersion was filtrated to obtain a flexible membrane. After that, the film was dried at 60 °C for 6.0 h. The sulfur was with a weight content of 45 wt% and an areal sulfur loading of 1.1 mg cm⁻² in the flexible paper electrode. 13-mm-diameter disks were punched as the working cathodes for lithium-sulfur cells.

The standard 2025 coin-type cells with two-electrode cell configuration were employed for electrochemical performance evaluation. The electrolyte was 1.0 mol L⁻¹ lithium bis(trifluoromethanesulfonyl)imide (LiTFSI) and 1 wt% lithium nitrate (LiNO₃) in dimethyl ether and 1,3-dioxolane (volume ratio 1:1). 1.0-mm-thick lithium metal foil was applied as the anode and the Celgard 2400 membranes were acted as the separator. The lithium-sulfur cells were assembled in an argon-filled glove-box. The CV were performed on Solartron 1470E electrochemical workstation within a voltage window of 1.6–3.0 V at a scan rate of 0.1 mV s⁻¹. The cyclic performance was collected by Neware multi-channel battery cyler within a voltage window of 1.8–2.8 V.

Structure characterizations

The structure of the interested electrodes was identified by an X-ray powder diffractometer (XRD, D8-Advance, Bruker, Germany). The morphology of GS, GS-S composites and CGS, CGF cathode were characterized by a transmission electron microscopy (TEM, JEM 2010, JEOL Ltd., Tokyo, Japan) at 120.0 kV and a field scanning electron microscopy (SEM, JSM 7401F, JEOL Ltd., Tokyo, Japan) at 5.0 kV. The sulfur ratio in the GS-S composites was determined by thermogravimetric analysis (TGA) using TGA/DSC1 STAR^e system in N₂ atmosphere with a temperature ramp rate of 20 °C min⁻¹. The Autosorb-iQ2-MP-C adsorption analyzer was employed to record the N₂ adsorption-desorption isotherms of the GS-S composites and CGS cathode at –196 °C. Before N₂ sorption isotherm measurements, the sample was degassed at a very low temperature of 50 °C until a manifold pressure of 2.0 mmHg was achieved to avoid the sulfur sublimation. The surface area was determined by the Brunauer-Emmett-Teller (BET) method, and the pore size distribution plot was calculated by the quenched-solid density functional theory using adsorption branch. Electrical conductivity was obtained by four-probe test of a disk with diameter of 13.0 mm punched from large-scale CGS paper. The mechanical tests of CGS electrode was collected on a GT-TS-2000 instrument at room temperature.

Acknowledgements

This work was supported by the Natural Scientific Foundation of China (No. 21306103, 21276141, 21273109, 21422604), and

the Research Fund for the Doctoral Program of Higher Education of China (20120002120047).

Appendix A. Supporting information

Supplementary data associated with this article can be found in the online version at <http://dx.doi.org/10.1016/j.nanoen.2014.11.062>.

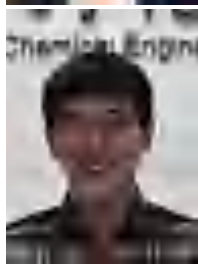
References

- [1] Z. Liu, J. Xu, D. Chen, G.Z. Shen, *Chem. Soc. Rev.* 44 (2015) 161–192.
- [2] H.L. Zhu, Z.Q. Fang, C. Preston, Y.Y. Li, L.B. Hu, *Energy Environ. Sci.* 7 (2014) 269–287.
- [3] G.M. Zhou, F. Li, H.M. Cheng, *Energy Environ. Sci.* 7 (2014) 1307–1338.
- [4] P.H. Yang, W.J. Mai, *Nano Energy* 8 (2014) 274–290.
- [5] Y.H. Hu, X.L. Sun, *J. Mater. Chem. A* 2 (2014) 10712–10738.
- [6] A. Manthiram, Y. Fu, S.-H. Chung, C. Zu, Y.-S. Su, *Chem. Rev.* 114 (2014) 11751–11787.
- [7] Y.X. Yin, S. Xin, Y.G. Guo, L.J. Wan, *Angew. Chem. Int. Ed.* 52 (2013) 13186–13200.
- [8] X.L. Ji, K.T. Lee, L.F. Nazar, *Nat. Mater.* 8 (2009) 500–506.
- [9] D.W. Wang, Q.C. Zeng, G.M. Zhou, L.C. Yin, F. Li, H.M. Cheng, I.R. Gentle, G.Q.M. Lu, *J. Mater. Chem. A* 1 (2013) 9382–9394.
- [10] Y. Yang, G.Y. Zheng, Y. Cui, *Chem. Soc. Rev.* 42 (2013) 3018–3032.
- [11] X.B. Cheng, J.Q. Huang, Q. Zhang, H.J. Peng, M.Q. Zhao, F. Wei, *Nano Energy* 4 (2014) 65–72.
- [12] Z. Yuan, H.-J. Peng, J.-Q. Huang, X.-Y. Liu, D.-W. Wang, X.-B. Cheng, Q. Zhang, *Adv. Funct. Mater.* 24 (2014) 6105–6112.
- [13] K.K. Jin, X.F. Zhou, L.Z. Zhang, X. Xin, G.H. Wan, Z.P. Liu, *J. Phys. Chem. C* 117 (2013) 21112–21119.
- [14] G.M. Zhou, D.W. Wang, F. Li, P.X. Hou, L.C. Yin, C. Liu, G.Q. Lu, I.R. Gentle, H.M. Cheng, *Energy Environ. Sci.* 5 (2012) 8901–8906.
- [15] Y. Zhao, W.L. Wu, J.X. Li, Z.C. Xu, L.H. Guan, *Adv. Mater.* 26 (2014) 5113–5118.
- [16] L.N. Wang, Y. Zhao, M.L. Thomas, H.R. Byon, *Adv. Funct. Mater.* 24 (2014) 2248–2252.
- [17] M.Q. Zhao, Q. Zhang, J.Q. Huang, G.L. Tian, J.Q. Nie, H.J. Peng, F. Wei, *Nat. Commun* 5 (2014) 3410.
- [18] Z. Wang, Y. Dong, H. Li, Z. Zhao, H. Bin Wu, C. Hao, S. Liu, J. Qiu, X.W. Lou, *Nat. Commun.* 5 (2014) 5002.
- [19] X. Yang, L. Zhang, F. Zhang, Y. Huang, Y. Chen, *ACS Nano* 8 (2014) 5208–5215.
- [20] Y.C. Qiu, W.F. Li, W. Zhao, G.Z. Li, Y. Hou, M.N. Liu, L.S. Zhou, F.M. Ye, H.F. Li, Z.H. Wei, S.H. Yang, W.H. Duan, Y.F. Ye, J.H. Guo, Y.G. Zhang, *Nano Lett.* 14 (2014) 4821–4827.
- [21] J.Q. Huang, X.F. Liu, Q. Zhang, C.M. Chen, M.Q. Zhao, S. M. Zhang, W.C. Zhu, W.Z. Qian, F. Wei, *Nano Energy* 2 (2013) 314–321.
- [22] S. Thieme, J. Bruckner, I. Bauer, M. Oschatz, L. Borchardt, H. Althues, S. Kaskel, *J. Mater. Chem. A* 1 (2013) 9225–9234.
- [23] L. Zeng, F. Pan, W. Li, Y. Jiang, X. Zhong, Y. Yu, *Nanoscale* 6 (2014) 9579–9587.
- [24] T. Xu, J.X. Song, M.L. Gordin, H. Sohn, Z.X. Yu, S.R. Chen, D.H. Wang, *ACS Appl. Mater. Interfaces* 5 (2013) 11355–11362.
- [25] J.Q. Huang, H.J. Peng, X.Y. Liu, J.Q. Nie, X.B. Cheng, Q. Zhang, F. Wei, *J. Mater. Chem. A* 2 (2014) 10869–10875.
- [26] Y. Zhang, Z. Bakenov, Y. Zhao, A. Konarov, Q. Wang, P. Chen, *Ionics* 20 (2014) 803–808.
- [27] G. Zhou, L. Li, C. Ma, S. Wang, Y. Shi, N. Koratkar, W. Ren, F. Li, H.-M. Cheng, *Nano Energy* 11 (2015) 356–365.
- [28] X. Jia, Y. Cheng, Y. Lu, F. Wei, *ACS Nano* 8 (2014) 9265–9273.

- [29] X. Jia, Y. Kan, X. Zhu, G. Ning, Y. Lu, F. Wei, *Nano Energy* 10 (2014) 344-352.
- [30] H.J. Peng, T.Z. Hou, Q. Zhang, J.Q. Huang, X.B. Cheng, M.Q. Guo, Z. Yuan, L.Y. He, F. Wei, *Adv. Mater. Interfaces* 1 (2014) 1400227.
- [31] S.M. Zhang, Q. Zhang, J.Q. Huang, X.F. Liu, W.C. Zhu, M. Q. Zhao, W.Z. Qian, F. Wei, *Part. Part. Syst. Char.* 30 (2013) 158-165.
- [32] H.J. Peng, J.Q. Huang, M.Q. Zhao, Q. Zhang, X.B. Cheng, X.Y. Liu, W.Z. Qian, F. Wei, *Adv. Funct. Mater.* 24 (2014) 2772-2781.
- [33] M.Q. Zhao, X.F. Liu, Q. Zhang, G.L. Tian, J.Q. Huang, W.C. Zhu, F. Wei, *ACS Nano* 6 (2012) 10759-10769.
- [34] N. Jayaprakash, J. Shen, S.S. Moganty, A. Corona, L.A. Archer, *Angew. Chem. Int. Ed.* 50 (2011) 5904-5908.
- [35] C.F. Zhang, H.B. Wu, C.Z. Yuan, Z.P. Guo, X.W. Lou, *Angew. Chem. Int. Ed.* 51 (2012) 9592-9595.
- [36] J. Liu, T.Y. Yang, D.W. Wang, G.Q.M. Lu, D.Y. Zhao, S.Z. Qiao, *Nat. Commun* 4 (2013) 2798.
- [37] B. Zhang, X. Qin, G.R. Li, X.P. Gao, *Energy Environ. Sci.* 3 (2010) 1531-1537.
- [38] Y. Zhang, Y. Zhao, Z. Bakenov, A. Konarov, P. Chen, *J Power Sources* 270 (2014) 326-331.
- [39] J.-S. Kim, T.H. Hwang, B.G. Kim, J. Min, J.W. Choi, *Adv. Funct. Mater.* 24 (2014) 5359-5367.
- [40] X.G. Han, Y.H. Xu, X.Y. Chen, Y.C. Chen, N. Weadock, J.Y. Wan, H.L. Zhu, Y.L. Liu, H.Q. Li, G. Rubloff, C.S. Wang, L.B. Hu, *Nano Energy* 2 (2013) 1197-1206.
- [41] J.Q. Huang, Q. Zhang, H.J. Peng, X.Y. Liu, W.Z. Qian, F. Wei, *Energy Environ. Sci.* 7 (2014) 347-353.
- [42] H. Peng, J. Liang, L. Zhu, J.-Q. Huang, X.-B. Cheng, X. Guo, W. Ding, W. Zhu, Q. Zhang, *ACS Nano* 8 (2014) 11280-11289.
- [43] C.M. Chen, Q. Zhang, M.G. Yang, C.H. Huang, Y.G. Yang, M.Z. Wang, *Carbon* 50 (2012) 3572-3584.



Lin Zhu is a master student in inorganic chemistry at the Department of Chemical Engineering in Qufu Normal University and also a visiting student in Department of Chemical Engineering, Tsinghua University, China. Her current research focuses on materials chemistry for nanocomposite cathode for lithium-sulfur battery.



Hong-Jie Peng gained his Bachelor's degree from Department of Chemical Engineering, Tsinghua University, P. R. China and is currently a Ph.D. candidate at Tsinghua University. His research interests focus on nanocarbon, advanced functional materials, high-performance lithium batteries, and novel energy storage devices.



Jiyuan Liang received his Ph.D degree from school of chemistry and chemical engineering, Nanjing University, China. His research interests are the synthesis chemistry, porous carbon materials preparation and their applications in energy storage, especially for supercapacitor and lithium-sulfur batteries.



Jia-Qi Huang received his Ph.D degree from department of chemical engineering, Tsinghua University, China. He was a visiting researcher in Prof. P.M. Ajayan's group at Rice University, USA in 2010. His research interests are the mass production of CNTs/graphene as well as their applications in energy conversion and storage, especially for Li-S batteries and Li ion batteries.



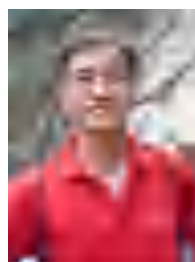
Cheng-Meng Chen received his Ph.D degree in materials science from Institute of Coal Chemistry, Chinese Academy of Sciences (ICC, CAS). From 2010 to 2011, he was a joint Ph.D student in Fritz Haber Institute of the Max Planck Society, Germany. Since July 2012, he was appointed as the group leader of Graphene & Renewable Energy Materials Group at ICC, CAS. He is currently engaged

in the research on chemically derived graphene and their applications in energy storage as well as thermal management.



Xuefeng Guo obtained his Bachelor's degree from Zhejiang University in 1995, and Ph.D. in Physical Chemistry from Nanjing University in 2000. After several-year postdoctoral research in Hong Kong Baptist University (2001-2002), and UMR 5253 CNRS, University of Montpellier II, France (2002-2003), he joined the faculty at Nanjing University at the end of 2003, where he

was appointed a professor of Chemistry in 2010. His research interests are mainly focused on novel low-dimensional nanomaterials and their applications in green catalysis and environment & energy-related fields.



Wancheng Zhu obtained his Bachelor's degree from Zhejiang University in 1995, Master's degree from Beijing University of Chemical Technology in 2002, and Ph.D in chemical engineering from Tsinghua University in 2008, followed by a postdoctoral fellowship in chemistry at Tsinghua University in 2012. In 2012, he was nominated as the head of the Department of Chemical

Engineering and appointed as a full professor of chemical engineering in 2013 at Qufu Normal University. His research interests are mainly focused on nano chemistry, crystal growth and design, catalysis, energy conversion and storage.



Peng Li obtained master degree in applied chemistry from He Bei University of Technology in 2005. He had worked in the field of lithium-ion battery in Tianjin Lishen and NEC (China) Co., Ltd, from 2005 to 2013. He is currently engaged in the research of battery and energy storage in Beijing Tsingna Technology Co., Ltd.



Qiang Zhang graduated in 2004 from the department of chemical engineering, Tsinghua University, China, where he continued doing research on mass production of carbon nanotubes and obtained his Ph.D in chemical engineering in 2009. After a short stay as a research associate in Case Western Reserve University, USA in 2009, he joined the Fritz Haber Institute of the Max Planck

Society, Germany as a post-doctoral fellow. He was appointed an associate professor of chemical engineering of Tsinghua University in 2011. His current research interests are hierarchical nanocarbon, lithium-sulfur batteries, and electrocatalysis.